Soft magnetic properties of FeCoSiBC amorphous alloys with high saturation magnetization

Hongxiang Cui[1,2] , Bangshao Dong[2,3,*], Yanxing Xing[2], Yun Cheng[1,*], Li Wang[1], and Shaoxiong Zhou[2]

[1] *School of Mechanical and Electrical Engineering, Shandong University (Weihai), Weihai 264209, China*

[2] *Jiangsu JITRI Advanced Energy Materials Research Institute Co., Ltd, Changzhou 213034, China*

[3] *Institute of Advanced Materials, North China Electric Power University, Beijing 102206, China*

ABSTRACT

To fulfill the demand of high saturation magnetization soft magnetic materials for electric motors, $Fe_{82-x}Co_xSi_4B_{13}C_1$ ($x = 0, 5, 10, 15, 20, 25$, and 30) amorphous alloys are prepared and effects of Co addition on soft magnetic properties and thermal parameters have been investigated. It shows that Curie temperature increases greatly with the increasing Co content. And the B_s of the low Co content amorphous alloys can be effectively enhanced. Especially, the amorphous alloy with 15 at% Co exhibits a high saturation magnetization of 1.73 T and a maximum permeability as high as 1.37×10^4 by appropriately annealed at 380 °C without magnetic fields for 10 min. Moreover, the relation between the coercivity and magnetic domain structure was investigated. The amorphous alloys are promising for further application in the field of electric motors.

1 Introduction

The Fe-based amorphous soft magnetic materials have attracted wide attention because of their high saturation magnetization (B_s), low coercivity (H_c), high permeability (μ), low core losses, high Curie temperature (T_c), and high glass forming ability (GFA) [1–4]. As a result, they have been widely used in electromagnetic devices such as inductors, transformers, and sensors [5–8]. However, B_s values of the commercial Fe-based amorphous alloys are merely 1.56 T for $Fe_{78}Si_9B_{13}$ [9] and 1.64 T for $Fe_{82}Si_4B_{13}C_1$ [10], which are much lower than the 1.9–2.1 T for the conventional Fe-Si electrical steels [11]. Thus, it is crucial to improve the B_s and

numerous efforts have been made to achieve this goal [12–16].

In the view of the alloy composition, the B_s of Fe-based amorphous alloys can be improved by increasing the Fe content [12, 14] and/or partially substituting Fe with Co [13–16]. However, it has been found that the GFA of the Fe-based amorphous alloys is weaken with the increasing Fe content. According to the Chaos principle [17], complex components make it difficult to precipitate complicated phases, and the competition between different phases can restrain the crystallization process. Therefore, the addition of Co can not only improve B_s, but also improve the GFA of the system. What's more, B_s and T_c are the intrinsic

Address correspondence to E-mail: dongbangshao@126.com; chy81@wh.sdu.edu.cn

E-mail Addresses: cuihongxiang1999@126.com

Springer

magnetic properties that depend on elementary composition and crystal structure. As accepted that the B_s of α-Fe(Co) phase (2.45 T) is higher than that of α-Fe phase (2.18 T) [18] and Co element exhibits higher B_s of 1394 K than Fe element (1043 K) [19]. Hence, the addition of Co is beneficial for enhancing GFA, B_s and T_c [20, 21].

Consequently, many efforts have been devoted to develop Fe- and Fe-Co based amorphous alloys. Kong et al. have developed a new amorphous Fe–P–B–Si–C alloy with high B_s of 1.70 T [22]. It has subsequently been reported that the partial replacement of Fe by Co causes a further increase in B_s to 1.74 T for $Fe_{68}Co_{15}P_3B_{11}Si_2C_1$ [16] and 1.76 T for $Fe_{68}Co_{17}P_3B_8Si_4$ [23]. However, the P-containing alloys show several disadvantages, such as the difficulty in controlling the alloy composition [24]. Therefore, there is a strong demand to develop P-free Fe-based amorphous alloys. Moreover, it should be noted that the Metglas 2605Co ($Fe_{67}Co_{18}B_{14}Si_1$) with high B_s of 1.80 T and low H_c of 2.0 A/m are only obtained by annealed at magnetic fields [19, 25], which cannot be applied in electric motors.

There is a large demand of high B_s and low core loss amorphous alloys without magnetic-fields annealing serving as the stator core in the field of electric motors. In this study, we try to improve the B_s of the famous commercially applied 2605HB1 [26] amorphous alloy by substituting Fe with Co. The $Fe_{82-x}Co_xSi_4B_{13}C_1$ ($x = 0$, 5, 10, 15, 20, 25 and 30) amorphous alloys are synthesized and effects of Co addition on soft magnetic properties and thermal parameters are explored.

2 Experiment

$Fe_{82-x}Co_xSi_4B_{13}C_1$ ($x = 0$, 5, 10, 15, 20, 25, and 30) alloys were prepared by melting the mixtures of pure Fe (99.99 wt%), Co (99.95 wt%), Si (99.99 wt%), pre-alloyed Fe-5% C and Fe-20% B in a highly purified argon atmosphere. And the ingots were re-melted to ensure the homogeneity. Amorphous ribbons with a width of 3 mm and thickness of 20 μm were prepared by single roller melt-spinning method with a wheel velocity of 29 m/s. The phase structure of both as-quenched and annealed ribbons was identified by X-ray diffraction (XRD, Bruker D8 Advance) with Cu-Kα radiation. Thermal parameters associated with crystallization was examined by differential scanning calorimetry (DSC, NETZSCH 404 C) at a heating rate

of 40 °C/min under an argon flow. Annealing treatment without magnetic fields was carried out at 280 to 440 °C for 10 min in a vacuum atmosphere under a low pressure of 2 Pa. The H_c and μ_m were tested by a DC B–H loop tracer (EXPH-100, Riken Denshi Co., Ltd) under a field up to 800 A/m. The B_s was measured with a vibrating sample magnetometer (VSM, Lake Shore 7410) under a field up to 800 kA/m. Additionally, the structure of magnetic domain was characterized via the Magneto-optical Kerr Microscope (MOKE, KMPL-Spin-X).

3 Results and discussion

The XRD patterns of $Fe_{82-x}Co_xSi_4B_{13}C_1$ ($x = 0$, 5, 10, 15, 20, 25, and 30) as-quenched ribbons are shown in Fig. 1. All patterns exhibit a wide peak near 44.5° without any sharp peak, indicating the amorphous structure of the samples.

Figure 2 shows the DSC curves measured at a heating rate of 40 °C/min of the as-quenched $Fe_{82-x}Co_xSi_4B_{13}C_1$ ($x = 0$, 5, 10, 15, 20, 25, and 30) alloy ribbons. All alloy ribbons exhibit two distinct exothermic peaks, which indicates the crystallization process involves two separated crystallization steps. The onset temperatures of the first and second exothermic peaks were denoted as T_{x1}, T_{x2}, respectively. And, T_{x1} presents a slight change which can be regarded as constant over the whole Co content range, while T_{x2} increases with increasing Co content. An endothermic
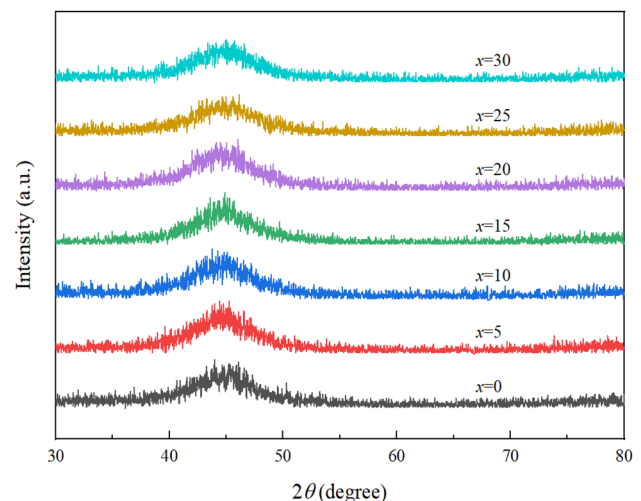

Fig. 1 XRD patterns of as-quenched $Fe_{82-x}Co_xSi_4B_{13}C_1$ ($x = 0$, 5, 10, 15, 20, 25, and 30) alloy ribbons
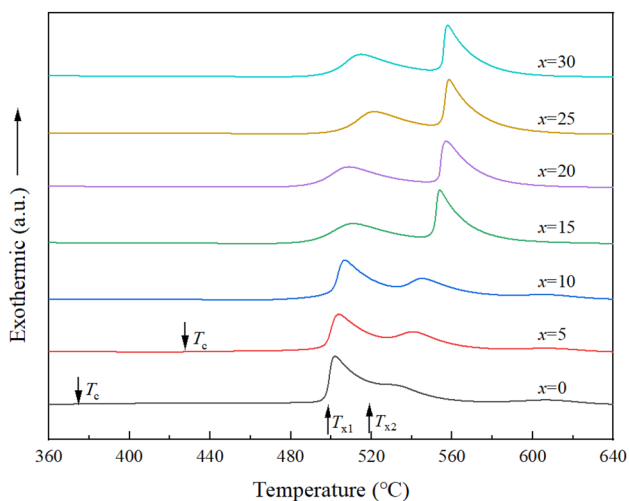
Fig. 2 DSC curves of the as-quenched $Fe_{82-x}Co_xSi_4B_{13}C_1$ ($x=0$, 5, 10, 15, 20, 25 and 30) alloy ribbons

Fig. 3 Annealing temperature dependent H_c of $Fe_{82-x}Co_xSi_4B_{13}C_1$ ($x=0$, 5, 10, 15, 20, 25, and 30) alloy ribbons

peak can be observed for the ribbons corresponding to the $x=0$ and 5 curves before the first exothermic peak, which has been proven to be the result of Curie transition from ferromagnetic state to paramagnetic state of the alloy ribbons. Whereas, no trace of T_c signal can be marked on the curves of $x=10$, 15, 20, 25 and 30 alloy ribbons, because the T_c exceeds the T_x and overlaps with the exothermic peak. This result indicates that T_c increases accordingly with the increasing of Co content, which is consistent with previous report [27]. An interesting phenomenon is that the intensity of the first exothermic peak is stronger than that of the second exothermic peak for the $Fe_{82-x}Co_xSi_4B_{13}C_1$ ($x=0$, 5 and 10) alloy ribbons. The reasons might be that (i) the ribbons with a higher melting temperature release more enthalpy during the initial crystallization reaction [28], (ii) in the Fe–Si–B–C system, when the Fe content exceeds 82 at%, the DSC curve exhibits two distinct exothermic peaks. However, as T_{x1} increases with decreasing Fe content, when Fe content drops to or below 82 at%, the two exothermic peaks tend to overlap [29]. What's more, T_{x2} increases with increasing Co content. Therefore, in the alloys studied in this paper, where there is either without Co or a small amount of Co, the two exothermic peaks tend to overlap into a single peak.

Variation of H_c with the annealing temperature for $Fe_{82-x}Co_xSi_4B_{13}C_1$ ($x=0$, 5, 10, 15, 20, 25, and 30) alloy ribbons after annealed for 10 min is shown in Fig. 3. On sees that for the alloy ribbons of Co free, the H_c firstly decreases to 5.9 A/m and then increases
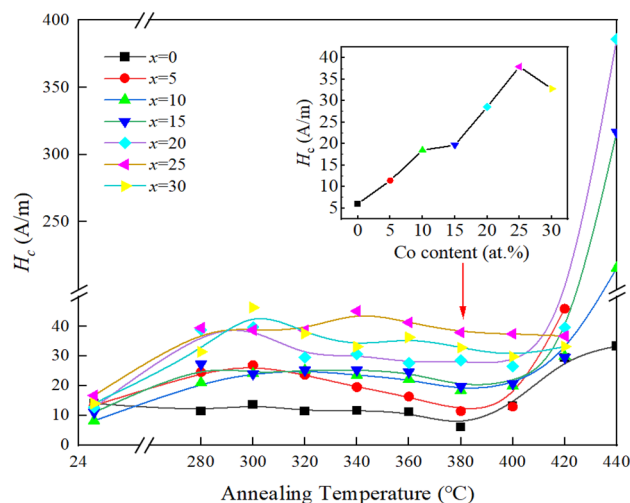
with the increasing annealing temperature. And the H_c can keep very low value (about 10 A/m) under the annealing temperature from 280 °C to 380 °C. However, the alloy ribbons with Co addition exhibit obviously different phenomenon. For the alloy ribbons of Co addition, the H_c maintains a high value more than 10 A/m and demonstrates a trend of first increasing, then decreasing and finally increasing with increasing annealing temperature. The H_c of all alloy ribbons reaches the minimum value after annealed at 380 °C for 10 min and the H_c at 380 °C exhibits a trend of first increasing and then decreasing with increasing Co content. In conclusion, with the increasing of Co content, the optimal H_c increases, while the optimum annealing temperature interval decreases.

Figure 4 shows the annealing temperature dependence of μ_m for $Fe_{82-x}Co_xSi_4B_{13}C_1$ ($x=0$, 5, 10, 15, 20, 25, and 30) alloy ribbons. In contrast to the tendency of H_c, the μ_m decreases with the increasing of Co content. On the one hand, the trend of the μ_m can be described as an initial increase, followed by a subsequent decrease for the $Fe_{82-x}Co_xSi_4B_{13}C_1$ ($x=0$, 5 and 10) alloy ribbons. On the other hand, the μ_m of the $Fe_{82-x}Co_xSi_4B_{13}C_1$ ($x=15$, 20, 25, and 30) alloy ribbons nearly keeps a constant value in the whole annealing temperature interval.

Based on the annealing temperature dependence of H_c and μ_m, Fig. 5 shows the hysteresis loops, soft magnetic properties and corresponding XRD patterns of the $Fe_{82-x}Co_xSi_4B_{13}C_1$ ($x=0$, 5, 10, 15, 20, 25, and 30) alloy ribbons after annealed at 380 °C for
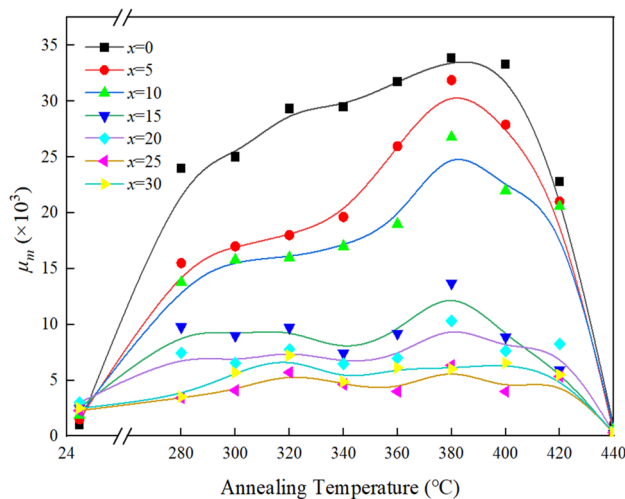
Fig. 4 Annealing temperature dependence of μ_m for $Fe_{82-x}Co_xSi_4B_{13}C_1$ ($x = 0, 5, 10, 15, 20, 25,$ and 30) alloy ribbons

10 min. One sees that from Fig. 5a, b that with the increase of Co, the B_s of the $Fe_{82-x}Co_xSi_4B_{13}C_1$ ($x = 0$, 5, 10, 15, 20, 25, and 30) alloy ribbons annealed firstly increase from 1.64 T for $x = 0$ to 1.73 T for $x = 15$, and then decrease to 1.63 T for $x = 30$. The arrows in Fig. 5c present the summit position of the amorphous broad diffraction peak. It is noteworthy that the peak in the XRD patterns shifts significantly to a lower angle until $x = 15$ and then shifts to the higher angle side with further increasing Co content. According to Bragg's Law [30], this shift indicates that the nearest neighbor atomic distance in the amorphous structure increases slightly with Co addition until $x = 15$, and then decreases with further increasing Co content. This compositional dependence has been interpreted a result of free electrons in the outer shell of the 15 at% Co amorphous alloy, which can contribute to the attainment of high B_s. This decrease in the number of free electrons in the outer shell can then contribute to the formation of metallic-like bonding among the constituent elements [31], which may be regarded as one of the reasons for the change in B_s.

In this section, we will discuss the possible reasons for the changes in magnetic properties. Previous studies [32] have shown that the destruction of B, P, and Si on the magnetic moment (m_s) in Fe-base amorphous increases successively. P, Si, and Ge are considered as substitutional elements, whereas B and C are interstitial elements. The mass density of substitutional elements decreases significantly when

they are added to the alloy, while the mass density of interstitial elements decreases less.

The relationship between the spontaneous magnetization (M_s) and the temperature (T) of amorphous ferromagnets can be treated with traditional effective molecular field approximation. For ferromagnet systems with two kinds of magnetic atoms, it can be expressed as follows [33],

$$M_s(T) = |m_{Fe}(T)\chi + m_{Co}(T)(1 - \chi)|, \tag{1}$$

where m_{Fe} and m_{Co} are the magnetic moment of Fe and Co, χ relates to the atomic spin quantum number and the exchange integral of the spin.

Due to the stronger exchange interaction between Fe–Co and Co–Co atoms compared to Fe–Fe atoms [34], the addition of Co atom increases the value of χ. For alloys without Co addition, $\chi < 1$, both terms on the right side of the equation are positive. With the increase of Co content, χ gradually increases and becomes greater than 1. At this point, the first term on the right side of the equation is positive, but the second term becomes negative. As a result, the absolute value of the sum of the two, M_s decreases.

The Slater-Pauling curve based on the rigid band model [35], also can explain the changes of B_s. According to this model, the m_s of $Fe_{70}Co_{30}$ is the largest. There are holes in both positive and negative spin bands in Fe. With the addition of Co, the excess d electrons enter the positive spin band with high state density, which increases the positive spin number and m_s. However, near 30 at% Co, the positive band is almost filled, then the d electrons begin to enter the negative band, and the m_s decreases with the increase of d electrons. The same trend was also found in amorphous Fe–Co–B alloys [36]. And the maximum value of B_s corresponding to 10–20 at% Co, which is consistent with conventional amorphous alloys.

The H_c of the amorphous alloys can be expressed as follows [37]:

$$H_c \propto (\delta/B_s)(K + 3/2\lambda_s\sigma), \tag{2}$$

where δ is thickness of domain wall, B_s is saturated magnetization, K is anisotropy constant, λ_s is saturated magnetostriction, σ is internal stress. Based on these relations, the lower H_c seems to be dominated by the release of internal stress. The internal stress would be gradually released with the increasing annealing temperature until the optimal temperature. However, higher annealing temperature can lead to the
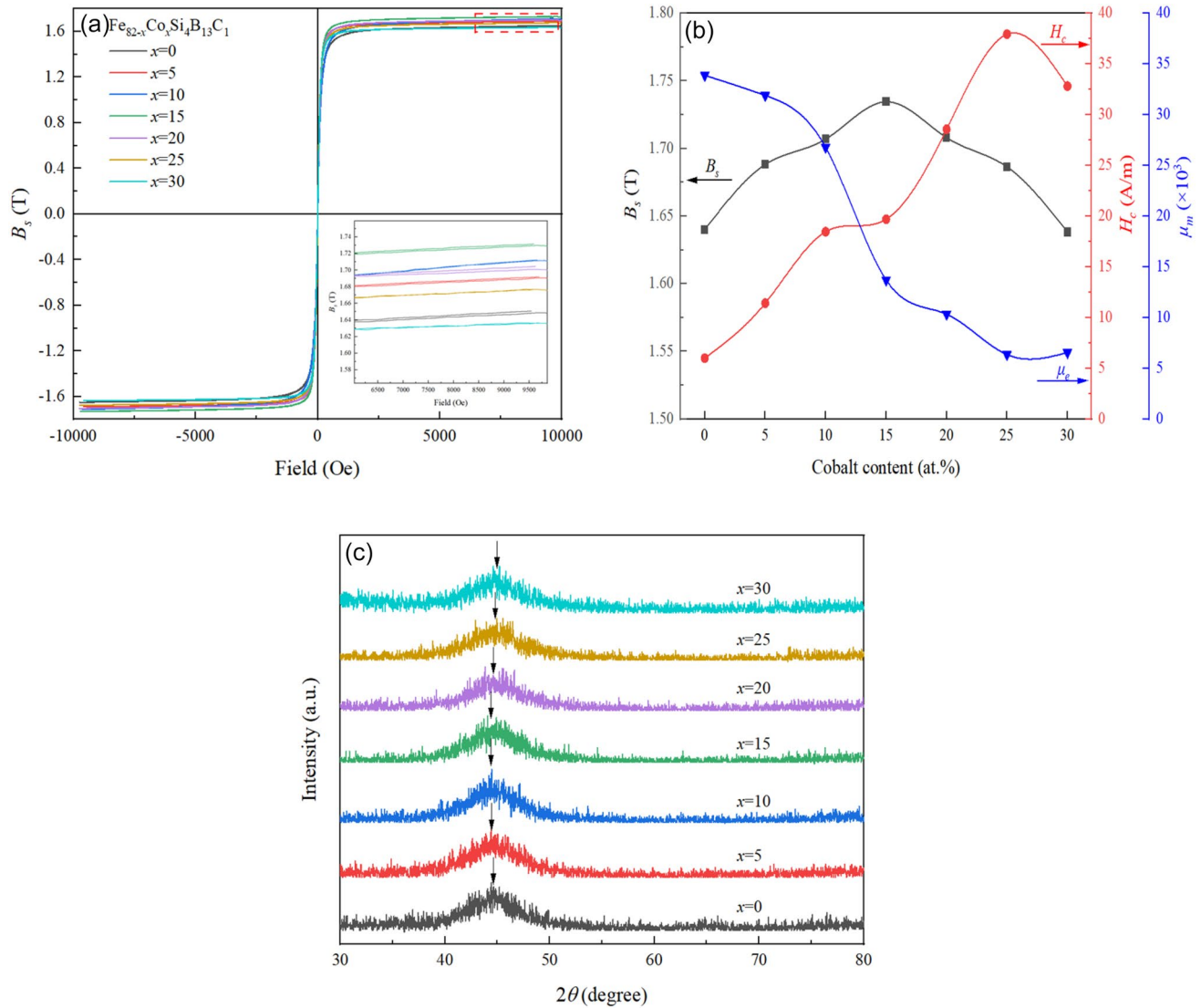
Fig. 5 **a** Hysteresis loops, **b** soft magnetic properties and **c** XRD patterns of $Fe_{82-x}Co_xSi_4B_{13}C_1$ ($x=0$, 5, 10, 15, 20, 25, and 30) alloy ribbons after annealed at 380 °C for 10 min

formation of crystalline phase, such as bcc-Fe, which increases the anisotropy and ultimately deteriorates the soft magnetic property.

A notable phenomenon observed is that there is a small hump for the H_c of alloy ribbons annealed at 300 °C with $x \geq 5$, which can be explained by the existence of induced anisotropy. When the annealing temperature is much lower than T_c, magnetic softness will not be achieved, and will even be worsened in high-T_c systems [38].

For further understanding soft magnetic properties, magnetic domains were examined. As shown

in Fig. 6, for the as-quenched $Fe_{82-x}Co_xSi_4B_{13}C_1$ alloy ribbons, the magnetic domains direction (see Fig. 6a, c, e) is almost in sensitive direction and all alloy ribbons exhibit small strips. The internal stress distributions within the strips differ due to the influence of the quench curing mode and heat treatment process, resulting in varying magnetoelastic energy and related induced uniaxial anisotropy (K_u) values. The magnetic anisotropy will directly affect the magnetic structure of amorphous crystals without grain boundaries and other defects. Due to the uniaxial properties of K_u, the domain walls in amorphous materials are mainly 180° (see in Fig. 6a–e) [39].

Fig. 6 Magnetic domains of $Fe_{82-x}Co_xSi_4B_{13}C_1$ ($x=0$, 15, and 30) alloy ribbons in as-quenched (**a**, **c**, and **e**) and annealed at 380 °C (**b**, **d,** and **f**)
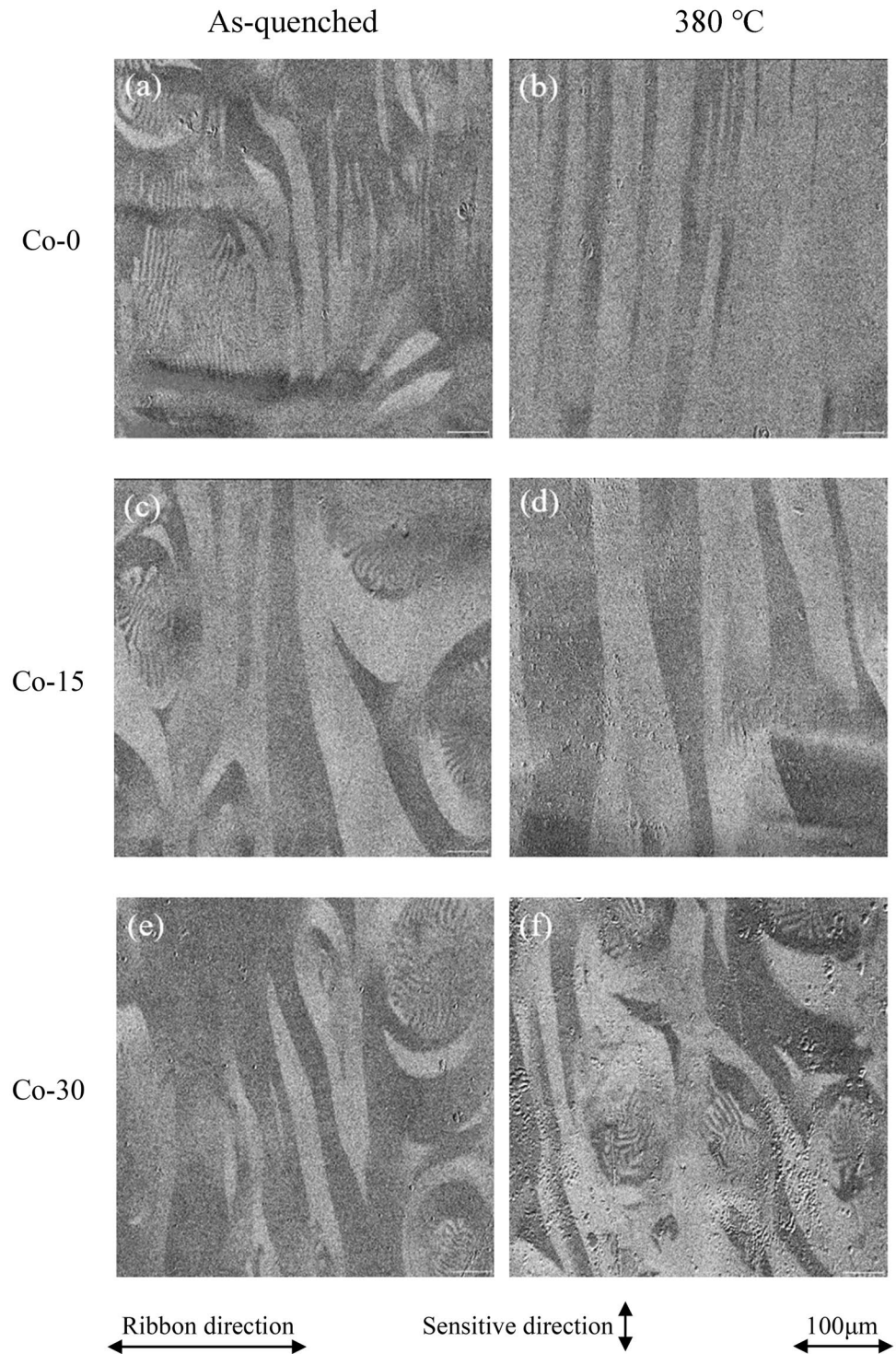
For alloy ribbons without Co, the domain direction and width is more uniform after annealing because of the release of internal stress. However, for 15 at% Co addition alloy ribbons, the annealing treatment makes the domains more wider. Co addition results in a large annealing induced anisotropy due to the well-known pair ordering effect where K_u becomes proportional to the square of Co content [40]. For 30 at% Co addition alloy ribbons, the domain structure does not become uniform so much as change

Table 1 Magnetic properties of typical soft magnetic alloys

Alloys	B_s (T)	H_c (A/m)
$Fe_{77}Co_5Si_4B_{13}C_1$	1.68	11.4
$Fe_{72}Co_{10}Si_4B_{13}C_1$	1.70	18.4
$Fe_{67}Co_{15}Si_4B_{13}C_1$	1.73	19.7
Fe-6.5wt%Si [41]	1.85	45.0
Fe-3.5wt%Si [25]	1.97	41.0
$Fe_{78}Si_9B_{13}$ [9]	1.56	2.6
2605Co $Fe_{67}Co_{18}B_{14}Si_1$ [19, 25]	1.80	2.0*

*Annealed at magnetic fields

into worse. After annealing, the magnetic domain structure changes from narrow to wide and then to disordered, indicating an increase in K_u and H_c. In summary, the domain structure makes a good explanation for the changes of soft magnetic properties.

Table 1 presents a summary of magnetic properties of the $Fe_{82-x}Co_xSi_4B_{13}C_1$ (x = 5, 10, and 15) amorphous ribbons, along with other representative alloys reported for comparison [9, 25, 41]. One sees from Table 1 that $Fe_{82-x}Co_xSi_4B_{13}C_1$ alloy ribbons exhibit a smaller H_c than the traditional non-oriented Fe–Si alloy but a larger B_s than $Fe_{78}Si_9B_{13}$, indicating that they can reduced both the core loss and the device volume. In contrast to Metglas 2605Co ($Fe_{67}Co_{18}B_{14}Si_1$), the $Fe_{82-x}Co_xSi_4B_{13}C_1$ alloy ribbons do not require the application of magnetic-fields annealing, making them promising for potential applications in the electric motors industry.

4 Conclusion

Effects of Co addition on thermal parameters and magnetic properties of $Fe_{82-x}Co_xSi_4B_{13}C_1$ (x = 0, 5, 10, 15, 20, 25, and 30) amorphous alloys are investigated. And origin of the changes in soft magnetic properties of these Co-doped FeSiBC amorphous alloys are explored. The results obtained can be summarized as follows:

1) B_s of $Fe_{82-x}Co_xSi_4B_{13}C_1$ amorphous alloys is effective enhanced from 1.64 T to 1.73 T with Co addition from 0 to 15 at%, and then decrease to 1.63 T with Co addition from 15 to 30 at%. T_c of $Fe_{82-x}Co_xSi_4B_{13}C_1$ amorphous alloys increases greatly. While H_c and μ_e deteriorated after Co addition.

2) The high B_s is contributed to the optimum Co/Fe content ratio with the maximum magnetic interaction. The magnetic domain structure changes from narrow to wide and then to disordered, indicating the increase in H_c.

3) Compared to the traditional materials, the $Fe_{82-x}Co_xSi_4B_{13}C_1$ amorphous alloys with more applicable H_c and B_s without the application of magnetic-fields annealing, making them highly suitable for potential applications in the field of electric motors.

Author contributions

HC: data curation, formal analysis, investigation, writing—original draft. BD: conceptualization, formal analysis, funding acquisition, supervision, writing—review and editing. YX: conceptualization, formal analysis, supervision. YC: visualization, supervision, writing—review and editing. LW: supervision, visualization. SZ: project administration, resources.

Data availability

Data will be made available on request.

Declarations

Conflict of interest The authors declare that they have no known competing financial interests or personal relationships that could have appeared to influence the work reported in this paper.

Ethical approval There are no experiments involving human tissue.

References

1. G. Herzer, H.R. Hilzinger, Recent developments in soft magnetic materials. Phys. Scripta (1988). https://doi.org/10.1088/00318949/1988/T24/003

2. R. Hasegawa, D. Azuma, Impacts of amorphous metal-based transformers on energy efficiency and environment. J. Magn. Magn. Mater. **320**(20), 2451–2456 (2008). https://doi.org/10.1016/j.jmmm.2008.04.052

3. T. Fukao, A. Chiba, M. Matsui, Test results on a super-high-speed amorphous-iron reluctance motor. IEEE Trans. Ind. Appl. **25**(1), 119–125 (1989). https://doi.org/10.1109/28.18881

4. C. Suryanarayana, A. Inoue, Iron-based bulk metallic glasses. Int. Mater. Rev. **58**(3), 131–166 (2013). https://doi.org/10.1179/1743280412Y. 0000 000007

5. D.C. Jiles, Recent advances and future directions in magnetic materials. Acta Mater. **51**(19), 5907–5939 (2003). https://doi.org/10.1016/j.actamat.2003.08.011

6. M.E. McHenry, M.A. Willard, D.E. Laughlin, Amorphous and nanocrystalline materials for applications as soft magnets. Prog. Mater. Sci. **44**(4), 291–433 (1999). https://doi.org/10.1016/S0079-6425(99)00002-X

7. B. Dong, Q. Zhi, D. Li et al., Abnormality of magnetic behavior and core loss of nanocrystalline $Fe_{73.5}Cu_1Nb_3Si_{15.5}B_7$ alloy. Sci. China Technological Sci. **53**, 343–347 (2010). https://doi.org/10.1007/s11431-010-0049-9

8. B. Dong, S. Zhou, J. Qin et al., The prediction of upper limit of copper content in CoBCu glass-forming alloys. Comput. Mater. Sci. **152**, 351–354 (2018). https://doi.org/10.1016/j.commatsci.2018.05.016

9. A. Datta, D. Nathasingh, R.J. Martis et al., Saturation and engineering magnetostriction of an iron-base amorphous alloy for power applications. J. Appl. Phys. **55**(6), 1784–1786 (1984). https://doi.org/10.1063/1.333477

10. F. Kuniyoshi, E. Oda, S. Nakajima et al., Magnetic materials for energy and resource saving. Hitachi Hyoron **95**(43), 48 (2013)

11. A. Inoue, F. Kong, Q. Man et al., Development and applications of Fe-and Co-based bulk glassy alloys and their prospects. J. Alloys Compd. **615**, S2–S8 (2014). https://doi.org/10.1016/j.jallcom.2013.11.122

12. H. Li, A. Wang, T. Liu et al., Design of Fe-based nanocrystalline alloys with superior magnetization and manufacturability. Mater. Today. **42**, 49–56 (2021). https://doi.org/10.1016/j.mattod.2020.09.030

13. R. Parsons, Z. Li, K. Suzuki, Nanocrystalline soft magnetic materials with a saturation magnetization greater than 2 T. J. Magn. Magn. Mater. **485**, 180–186 (2019). https://doi.org/10.1016/j.jmmm.2019.04.052

14. A. Wang, C. Zhao, H. Men et al., Fe-based amorphous alloys for wide ribbon production with high *Bs* and outstanding amorphous forming ability. J. Alloys Comp. **630**, 209–213 (2015). https://doi.org/10.1016/j.jallcom.2015.01.056

15. C. Parra, F.J. Bolivar, Effect of cobalt addition on the microstructural evolution, thermal stability and magnetic properties of Fe-based amorphous alloys. Vacuum **169**, 108911 (2019). https://doi.org/10.1016/j.vacuum.2019.108911

16. C. Zhao, A. Wang, A. He et al., Correlation between soft-magnetic properties and T_{x1}-T_c in high *bs* FeCoSiBPC amorphous alloys. J. Alloys Compd. **659**, 193–197 (2016). https://doi.org/10.1016/j.jallcom.2015.11.044

17. A.L. Greer, Confusion by design. Nature. **366**(6453), 303–304 (1993). https://doi.org/10.1038/366303a0

18. H. Ohno, Properties of ferromagnetic III–V semiconductors. J. Magn. Magn. Mater. **200**(1–3), 110–129 (1999). https://doi.org/10.1016/S0304-8853(99)00444-8

19. F. Wang, A. Inoue, Y. Han et al., Excellent soft magnetic Fe–Co–B-based amorphous alloys with extremely high saturation magnetization above 1.85 T and low coercivity below 3 A/m. J. Alloys Compd. **711**, 132–142 (2017). https://doi.org/10.1016/j.jallcom.2017.03.341

20. B. Shen, A. Inoue, C. Chang, Superhigh strength and good soft-magnetic properties of (Fe, Co)–B–Si–Nb bulk glassy alloys with high glass-forming ability. Appl. Phys. Lett. **85**(21), 4911–4913 (2004). https://doi.org/10.1063/1.1827349

21. C.D. Jr Graham, T. Egami, Magnetic properties of amorphous alloys. Annu. Rev. Mater. Sci. **8**(1), 423–457 (1978). https://doi.org/10.1146/annurev.ms.08.080178.002231

22. F. Kong, C. Chang, A. Inoue et al., Fe-based amorphous soft magnetic alloys with high saturation magnetization and good bending ductility. J. Alloys Compd. **615**, 163–166 (2014). https://doi.org/10.1016/j.jallcom.2014.06.093

23. Y. Han, J. Ding, F. Kong et al., FeCo-based soft magnetic alloys with high *bs* approaching 1.75 T and good bending ductility. J. Alloys Compd. **691**, 364–368 (2017). https://doi.org/10.1016/j.jallcom.2016.08.250

24. S. Banya, N. Maruyama, S. Fujino, Vapor pressure of phosphorus in liquid Fe–P alloys. Tetsu-to-Hagane **68**, 269–276 (1982). https://doi.org/10.2355/tetsutohagane955.68.2_269

25. F. Wang, A. Inoue, Y. Han et al., Soft magnetic Fe-Co-based amorphous alloys with extremely high saturation magnetization exceeding 1.9 T and low coercivity of 2 A/m[J]. J. Alloys Compd. **723**, 376–384 (2017). https://doi.org/10.1016/j.jallcom.2017.06.192

26. C.H. Hsu, Y.H. Chang, (2009) Impacts of Fe-based amorphous HB 1 core transformers on energy efficiency and environment protection. WSEAS International Conference. Proceedings. Mathematics and Computers in Science and Engineering. World Scientific and Engineering Academy and Society.

27. Y. Xing, B. Dong, S. Zhou et al., Soft magnetic properties of co-doped FeSiBC amorphous and nanocrystalline alloys. J. Magn. Magn. Mater. **565**, 170249 (2023). https://doi.org/10.1016/j.jmmm.2022.170249

28. Z. Zhu, H. Zhang, H. Wang, B. Ding, Z. Hu, Influence of casting temperature on the thermal stability of Cu- and Zr-based metallic glasses: theoretical analysis and experiments. J. Mater. Res. **23**(10), 2714–2719 (2008). https://doi.org/10.1557/JMR.2008.0335

29. C. Dong, A. Inoue, X. Wang et al., Soft magnetic properties of $Fe_{82-83}B_{14-15}Si_2C_{0.5-1}$ amorphous alloys with high saturation magnetization above 1.7 T. J. Non-cryst. Solids. **500**, 173–180 (2018). https://doi.org/10.1016/j.jnoncrysol.2018.07.072

30. C.J. Humphreys, The significance of Bragg's law in electron diffraction and microscopy, and Bragg's second law. Acta Crystallogr. Sect. A: Found. Crystallogr. **69**(1), 45–50 (2013). https://doi.org/10.1107/S0108767312047587

31. G. Herzer, Modern soft magnets: amorphous and nanocrystalline materials. Acta Mater. **61**(3), 718–734 (2013). https://doi.org/10.1016/j.actamat.2012.10.040

32. A. Makino, T. Kubota, C. Chang, M. Makabe, A. Inoue, Fe-metalloids bulk glassy alloys with high Fe content and high glass-forming ability. J. Mater. Res. **23**(5), 1339–1342 (2008). https://doi.org/10.1557/JMR.2008.0180

33. L. Hou, M. Li, C. Jiang et al., Thermal and magnetic properties of Fe (Co) BCCu amorphous alloys with high saturation magnetization of 1.77 T. J. Alloys Compd. **853**, 157071 (2021). https://doi.org/10.1016/j.jallcom.2020.157071

34. J.M. MacLaren, T.C. Schuthess, W.H. Butler, R. Sutton, M. McHenry, Electronic structure, exchange interactions, and Curie temperature of FeCo. J. Appl. Phys. **85**, 4833–4835 (1999). https://doi.org/10.1063/1.370036

35. A. Díaz-Ortiz, R. Drautz, M. Fähnle et al., Structure and magnetism in bcc-based iron-cobalt alloys. Phys. Rev. B **73**(22), 224208 (2006). https://doi.org/10.1103/PhysRevB.73.224208

36. R.C. O'Handley, R. Hasegawa, R. Ray et al., Ferromagnetic properties of some new metallic glasses. Appl. Phys. Lett. **29**(6), 330–332 (1976). https://doi.org/10.1063/1.89085

37. T. Bitoh, A. Makino, A. Inoue, Origin of low coercivity of Fe-(Al, Ga)-(P, C, B, Si, Ge) bulk glassy alloys. Mater. Trans. **44**(10), 2020–2024 (2003). https://doi.org/10.2320/matertrans.44.2020

38. C. Zhao, A. Wang, S. Yue et al., Significant improvement of soft magnetic properties for Fe (Co) BPSiC amorphous alloys by magnetic field annealing. J. Alloys Compd. **742**, 220–225 (2018). https://doi.org/10.1016/j.jallcom.2018.01.311

39. A. Hubert, R. Schäfer, *Magnetic Domains* (Springer, Berlin, 1998), p.255

40. K. Suzuki, R. Parsons, B. Zang et al., Nanocrystalline soft magnetic materials from binary alloy precursors with high saturation magnetization. AIP Adv. **9**(3), 035311 (2019). https://doi.org/10.1063/1.5079778

41. A. Inoue, F.L. Kong, Q.K. Man et al., Development and applications of Fe-and Co-based bulk glassy alloys and their prospects. J. Alloys Compd. **615**(S2), S8 (2014). https://doi.org/10.1016/j.jallcom.2013.11.122